Multidisciplinary | Rapid Review | Open Access Journal

Date of publication xxxx 00, 0000, date of current version xxxx 00, 0000.

Digital Object Identifier 10.1109/ACCESS.2017.Doi Number

Modular Tri-port Converter for Switched Reluctance Motor based Hybrid Electrical Vehicles

Tianhao Wu[1], Wei Li[2], Kai Ni[1], Student Member, IEEE, Sen Song[1], and Mohammed Alkahtani[1]

[1]Department of Electrical Engineering and Electronics, University of Liverpool, Brownlow Hill, Liverpool, L69 3GJ, United Kingdom
[2]State Grid International Development Co., Ltd, No.8 Xuanwumenneni Street, Xicheng District, 100031, Beijing, China

Corresponding author: Kai Ni (e-mail: k.ni@student.liverpool.ac.uk).

ABSTRACT Hybrid electrical vehicle (HEV) is a popular transport solution to reducing carbon dioxide emissions. Switched reluctance motors (SRMs) are one of the most promising motors for such applications. In SRM-based series type HEV, there are three energy components, i.e., generator, battery bank, and SRM. A tri-port converter is needed to combine the three energy components in one power converter. The tri-port converter has a modular and concise structure, which meets the requirements for HEV applications. The proposed tri-port converter supports five working modes, including generator to SRM, battery bank to SRM, generator and battery bank to SRM, generator to SRM and battery bank, and battery bank to SRM and generator under driving conditions; under standstill conditions, generator to battery bank and battery bank to generator energy flow can also be realized without requiring extra converters. The corresponding control strategies are also developed to cooperate with different working modes. Moreover, the fault tolerance characteristics of the tri-port converter are investigated to expand its feasibility under harsh HEV application conditions. The simulation and experiments are undertaken with a 750W prototype to evaluate the performance of the proposed tri-port converter for HEV applications.

INDEX TERMS Tri-port, hybrid electric vehicles, SRM, fault tolerance.

I. INTRODUCTION

Currently, in order to decrease CO_2 emission, hybrid electric vehicles (HEV) is an effective solution [1-14]. Thanks to the features of no rare-earth metal, wide torque-speed range, robust structure and low cost, switched reluctance motor (SRM) is an available option for HEV application [15-24]. In [18], a test machine was constructed to prove that SRM is promising for HEV applications.

For HEV, there are three main energy components, namely, a battery, a motor, and a generator. In order to support flexible energy flows, several power electronics converters are needed, as shown in in Fig.1, in which B stands for battery bank, M stands for SRM, and G stands for generator/starter. Specifically, B-M means that the battery bank supplies energy to the drive motor alone; M-B means the motor recycles energy to the battery bank; G-M means the generator supplies energy to the drive motor alone; currently, some HEV integrates the generator and starter in one motor. Therefore, the battery needs to supply energy to the generator to start the internal combustion engine (ICE), which is B-G [25]. G-B means that the generator charges the battery bank under HEV standstill conditions. G-M-B stands for the case that the generator supplies energy to the motor and charges the battery at the same time. B-G refers to the situation that the battery bank supplies energy to the generator to start ICE. For M-G-B, the motor releases energy to the generator and battery bank in the braking condition. In order to simplify the system structure, a tri-port converter is needed to combine the generator, battery, and motor in one converter, through which flexible energy flow states are realized. In addition to the function requirements for flexible energy flow, the modular structure and simple power electronics topology are also the basis for electric powertrains of HEV to achieve massive production. Therefore, it is an urgent task to develop a power electronics converter with the aforementioned characteristics.

Currently, many topologies have been proposed for SRM based EVs/HEVs [2], [26-30]. Paper [2] presents an advanced three-phase 12/8 SRM drive system with integrated charging functions to enhance the market adoption of plug-in

HEVs. However, in this converter, the battery bank terminal voltage should match ICE generator output voltage, which decreases the system design flexibility. Paper [26] developed an integrated driving/charging SRM drive with a front-end converter for EVs to achieve plug-in charging, which does not have the tri-port function. In paper [27], by adding a passive circuit to the front-end of a conventional asymmetric converter, the new converter can boost the dc-link voltage for a high negative bias in the demagnetization mode. However, this topology is only used for the driving function. In paper [28], a dual source drive topology for SRM was studied, which allows an SRM to operate from ac mains or a low voltage battery supply, without applying a transformer to match the two voltage levels. However, the converter structure is relatively complex.

Another low-cost battery powered SRM drive with driving and charging functions was also proposed in [29]. Its battery charging is achieved through the motor windings without external transformers or other charging units. Due to the non-modular structure, the converter cannot be used in HEV. In order to obtain the characteristics of fast current build up and suitable demagnetization, a power converter with the functions of increased excitation and demagnetization voltages was designed by using an additional capacitor for high-speed operations [30]. Nevertheless, it is only used for the driving mode. Similarly, paper [31] proposed a four-level converter for SRM driving system to achieve fast demagnetization. Although the above mentioned state-of-the-art research has developed a lot of driving topologies for SRM driving or driving and charging integration topology, none of them can stratify the function presented in Fig.1.

In this paper, a novel converter with the characteristics of tri-port and modular structure is proposed. The proposed topology can support all the six working modes in Fig.1 almost without changing the traditional driving topology of SRM. Moreover, the proposed converter has the fault tolerance function, which can block the fault point to achieve fault tolerance operation. In this paper, the proposed tri-port converter and the corresponding working modes are illustrated in section II; section III presents the control strategy; the fault tolerance characteristics are discussed in section IV; simulation and experiment are also presented to verify the correction of the proposed topology in section V. The conclusion is given in the final part.

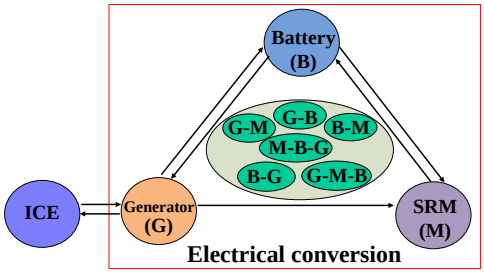

FIGURE 1. Desired energy flow modes

II. TRI-PORT CONVERTER AND OPERATION MODES

A. PROPOSED TRI-PORT CONVERTER

Fig. 2 presents the proposed converter and its deduction progress. In Fig.2, S_1~S_8 are MOSFETs; D_1~D_8 are diodes; J_1, J_2 and J_3 are the relays that are used for fault tolerance operation. There are three ports for the proposed converter: the first port is connected with the generator, and the second port is connected with the battery tank. The first and second ports are combined by a front-end three-level DC-DC converter, as shown in Fig.2 (a). V_1 and V_2 are the voltages of generator (G) and battery bank (B), respectively. The third port is SRM, and the corresponding drive topology is a traditional asymmetrical half bridge, as shown in Fig. 2(b), in which N_a, N_b and N_c are the central tapped nodes that can be achieved without any change in the SRM body structure. L_{a12} and L_{a34} are the windings of phase A of SRM, as shown in Fig.2 (c); similarly, L_{b12} and L_{b34} are the windings of phase B of SRM; L_{c12} and L_{c34} are the windings of phase C of SRM. The phase winding nodes are linked with the front-end three-level converter by a relay. The whole proposed topology is illustrated in Fig. 2 (d).

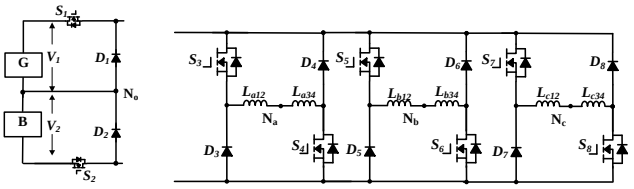

(a) Front-end three-level converter (b) Traditional asymmetrical half bridge

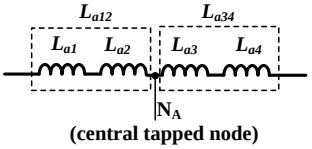

(c) Phase winding with central tapped node

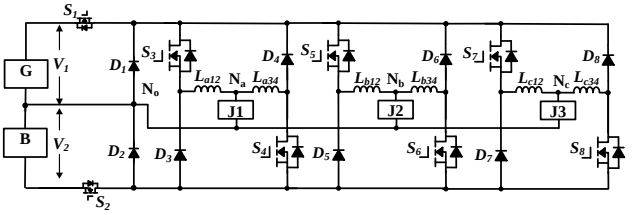

(d) Proposed multi-level and fault tolerance driving topology for SRM

FIGURE 2. Proposed SRM driving topology

The proposed topology has a modular structure that is convenient for massive production. As shown in Fig.3, the proposed topology is composed of eight modules, in which one diode and one switching device forms a module.

Compared with a traditional asymmetrical half bridge driving topology for SRM, only two extra modules are added.

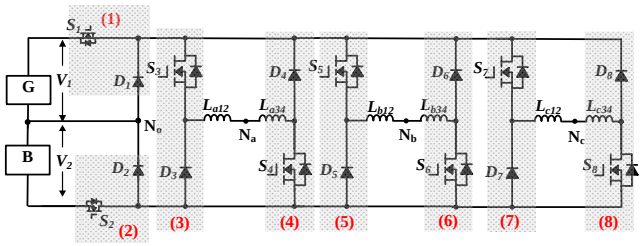

FIGURE 3. **Modular structure of proposed converter**

B. TOPOLOGY WORKING STATES

In the proposed topology, there are different working states for different energy flow modes. When both the generator and battery bank are working, by controlling the switching devices S_1 and S_2, there are three excitation modes that can be achieved, as shown in Fig.4. In Fig.4 (a), S_1 is conducted, and only the generator supplies energy to the motor; in Fig.4 (b), conducting S_2, only the battery bank supplies energy to the motor. By conducting both S_1 and S_2, the generator and battery bank supply energy to the motor at the same time. By controlling S_1 and S_2, three voltage levels can be achieved, which are V_1, V_2 and V_1+V_2, respectively. In the proposed topology, there are two demagnetization modes. Fig. 5 (a) presents a freewheeling mode, and Fig.5 (b) presents the case where energy recycles to the generator and battery bank.

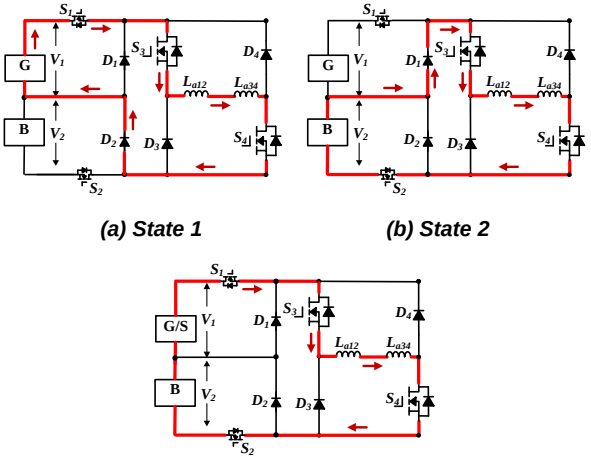

(a) State 1 *(b) State 2*

(c) State 3

FIGURE 4. **Excitation working states**

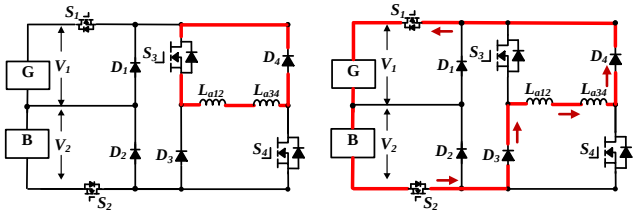

(a) Freewheeling *(b) Energy recycling*

FIGURE 5. **Demagnetization working states**

When an HEV is working in the standstill mode, the generator only needs to supply energy to the battery bank. The proposed converter works as a DC-DC converter. In Fig. 6, switching on J_1, J_2 and J_3; for phase-A, S_1 and S_3 are turned on, and the generator charges SRM phase inductor, as illustrated in Fig. 6 (a); and then, turn off S_1 and S_3, and turn on S_2 to discharge the energy in SRM phase inductance to the battery bank, as shown in Fig.6 (b).

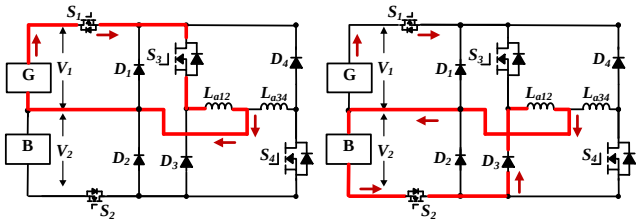

(a) G-B state 1 *(b) G-B state 2*

FIGURE 6. **Working states under standstill condition**

When the HEV is in the standstill mode, the battery bank supplies energy to the generator/starter to start the ICE. There are two working states in this progress. In Fig. 7, switching on J_1, J_2 and J_3; for phase-A, by turning on S_2 and S_4, the battery bank charges SRM phase inductor, as illustrated in Fig. 7 (a); and then, turn off S_2 and S_4, turn on S_1 to make the SRM phase inductance discharge energy to the generator, whose working state is shown in Fig.7 (b).

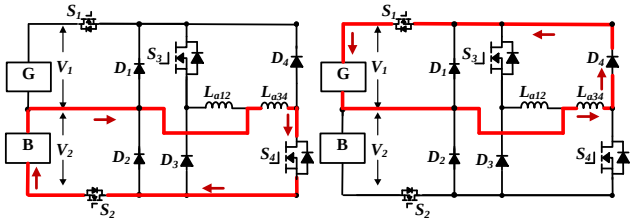

(a) B-G state 1 *(b) B-G state 2*

FIGURE 7. **Energy supply to generator working states**

All the six power flow modes shown in Fig.1 can be realized in the working states discussed above. The following chapter will illustrate the control strategies for the six power flow modes.

C. BATTERY BANK CHARGING

The battery bank can be charged in driving and standstill conditions. When the vehicle is in the driving condition, only the generator is employed to excite the windings of SRM, as shown in Fig.4 (a); during the demagnetization process, the battery bank can be charged, and the corresponding state is shown in Fig.5 (b). When the vehicle is in the standstill condition, the winding of SRM and the drive circuit will work as a DC-DC converter to transfer the power from the generator to battery bank, the corresponding working states are presented in Fig.(6).

III. CONTROL STRATEGY FOR THE PROPOSED TRI-PORT CONVERTER

As mentioned in Fig.1, there are six energy flow modes. Among these energy flow modes, there are two categories. The first one is the two-port energy flow mode, including G-M, B-M, B-G and G-B. The second one is the three-port energy flow mode, where G-B-M and M-G-B belong to this mode.

A. TWO-PORT ENERGY FLOW CONDITION

1) CONTROL STRATEGY FOR DRIVING MODE

G-M and B-M are the driving modes under two-port flow condition. When the proposed multi-port converter is in SRM driving mode, the system topology is equivalent to the traditional SRM driving topology; the voltage-PWM control and current chopping control (CCC) are adopted as the two basic control schemes. According to the given speed ω^*, the controller works in CCC mode under low speed condition, and it works in voltage-PWM control mode under high speed condition. The whole control block diagram is presented in Fig.8. The classical proportional integral (PI) is used in the speed controller, which is used to regulate the SRM speed. The encoder gives the SRM rotor position information, and the corresponding motor speed can be calculated by using a micro-controller. In the CCC strategy, the phase current is the control variable. The phase currents are measured by current sensors, and the current reference (i^*) is derived from the speed controller. The hysteresis controller is employed to generate the driving signals for the switching devices. In the voltage-PWM control system, the phase voltage is the control variable. According to the speed error, the effective phase voltage is controlled by the duty ratios of switching devices.

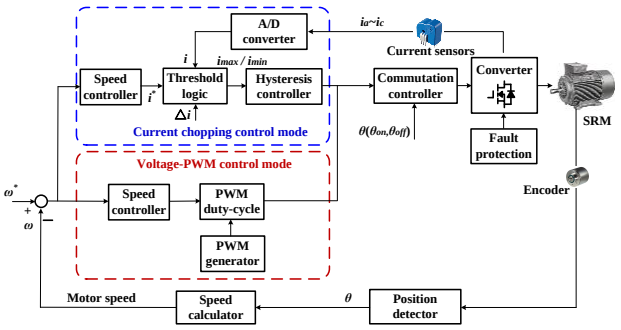

FIGURE 8. **SRM control strategy under driving mode**

2) CONTROL FOR STANDSTILL ENERGY EXCHANGE

B-G and G-M are included in the standstill energy exchange mode. When HEV is in the standstill battery charging mode (G-B) or standstill generator starting mode (B-G), the proposed tri-port converter needs to work as a DC-DC converter to transfer energy from one component to the others. In order to achieve a high power level, the three phases work in the parallel mode. Fig.9 indicates the control block scheme. Fig.9 (a) illustrates the control block diagram of battery bank supplying energy to generator; Fig.9 (b) illustrates the standstill battery charging control block diagram.

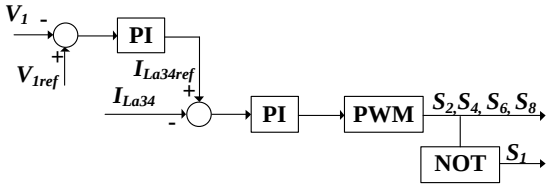

(a) Control diagram for HEV standstill generator starting

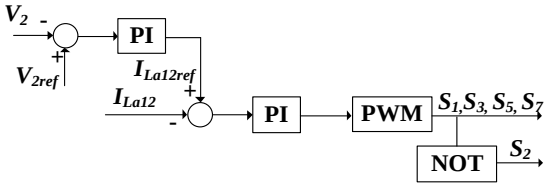

(b) Control diagram for HEV standstill battery charging

FIGURE 9. **HEV standstill energy exchange control**

B. THREE-PORT ENERGY CONTROL STRATEGY

When applying G-B-M, the generator output energy and the motor and battery bank input energy exist in both the battery charging and generator starting modes, where the energy is decoupled by SRM. The turn-on angle θ_{on} and turn-off angle θ_{off} of phase converter can be employed as the control variables to achieve energy control under the situation of energy decoupling. The other kind of three-port energy flow is M-B-G that has the same state of energy recycling of phase current, as is shown in Fig.10.

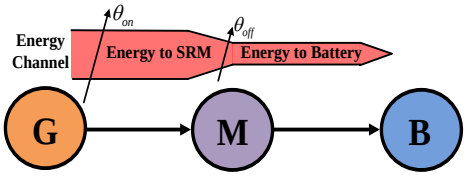

FIGURE 10. **Control strategy for three-port (G-M-B) energy exchange**

IV. FAULT TOLERANCE CONTROL BASED ON PROPOSED MULTI-PORT CONVERTER

Under the harsh application condition of EV and HEV, the SRM driving system is prone to fault, such as open circuit or short circuit of switching devices and phase windings. In a traditional three-phase asymmetrical half bridge topology, when one of the components is in open circuit, the faulty bridge arm cannot work, and the whole converter is under phase absence working condition. The corresponding torque ripple will increase obviously. By contrast, the proposed converter has fault tolerance characteristics that can realize fault tolerant operation. The proposed converter can block both the short-circuit and open-circuit points.

A. FAULT DIAGNOSIS AND FAULT TOLERANCE

Due to the harsh operation condition, the solid state devices suffer from short-circuit and open-circuit faults, as well as the phase windings.

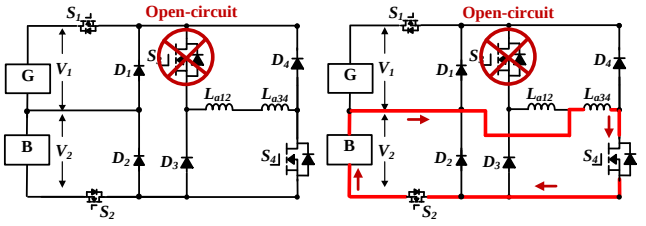

(a) Left part open-circuit fault (b) Left part fault tolerance working state 1

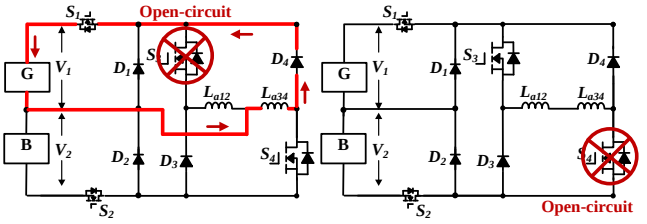

(c) Left part fault tolerance working state 2 (d) Right part open-circuit fault

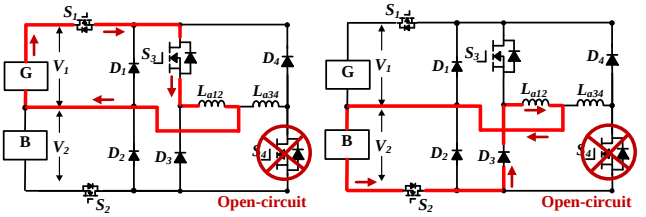

(e) Right part fault working state 1 (f) Right part fault working state 2

FIGURE 11. Fault tolerance operation

Fig.11 shows a typical example of single switch open-circuit fault. By switching on J_1, the battery bank and the right part of the faulty phase converter form a new converter to achieve fault tolerance operation when the left part of the converter fails. The corresponding operation states are shown in Fig.11 (b) and (c). In Fig.11 (b), switching on S_2 and S_4, in this state, the phase winding L_{a34} is excited. The energy recycling loop is presented in Fig.11 (c), in which S_4 is turned off, and the energy in L_{a34} is recycled to the generator. By forming the fault tolerance topology, the faulty part can be blocked. Similarly, when the faulty phase converter is with open-circuit fault in the right part, as shown in Fig.11 (d), by switching on relay J_1, the fault tolerance topology can be formed. The corresponding fault tolerance working states are presented in Fig.11 (e) and (f). In Fig.11 (e), switching on S_3, in this state, the phase winding L_{a12} is excited and produces a torque. The energy recycling loop is presented in Fig.11 (f), in which S_3 is turned off, S_2 is turned on, and the energy in L_{a12} is recycled to the generator. In the fault tolerance topology, the switching devices S_1 and S_2 can be turned on all the time, which will not influence the power supply to healthy phases. Because the proposed fault tolerance can block the faulty part, the fault tolerance topology under short-circuit fault is the same as that under open-circuit fault. Therefore, for the fault diagnosis strategy, only the fault location information is needed. The fault diagnosis flowchart for one phase is presented in Fig.12. As illustrated in Fig.12, when phase-A current is always equal to or over zero, by switching on J_1 and switching off S_3, if there is a current in phase A, or the phase-A current can decrease to zero, the left part is faulty, otherwise the right part fault is encountered. Since each phase converter operates independently, the fault diagnosis strategy and fault tolerance operation can also be applied in other phases. For switching devices S_1 and S_2, the press pack switching devices can be employed. When press pack switching devices under fault condition are equivalent to a short circuit, the power supply will not be influenced.

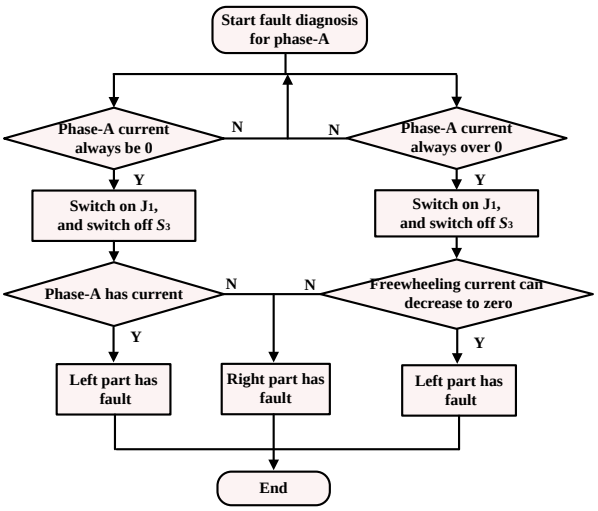

FIGURE 12. Flowchart of fault diagnosis

B. SRM MODELING UNDER FAULT TOLERANCE OPERATION

In normal operation, the phase voltage balance is given by:

$$\pm U_{dc} = Ri + L(\theta)\frac{di}{dt} + i\omega\frac{dL(\theta)}{d\theta} \tag{1}$$

where U_{dc} is the phase voltage of SRM, R is the SRM phase resistance, L is the phase inductance, i is the SRM phase current, θ is the SRM rotor angular position, and ω is the SRM angular speed. Due to the dual salient structure, the SRM phase inductance changes with the rotor position.

The SRM electromagnetic torque can be written as

$$T_e = \sum_{k=1}^{m} T_k = \sum_{k=1}^{m} \frac{1}{2} i_k{}^2 \frac{dL_k(\theta)}{d\theta} \tag{2}$$

where m is the motor phase, T_k is the phase instantaneous electromagnetic torque.

The mechanical motion equation of the SRM is given by:

$$J\frac{d\omega}{dt}+B\omega=T_e-T_l \tag{3}$$

where J is the combined moment of inertia of the motor and load, B is the combined friction coefficient of the motor and load, and T_l is the load torque.

When the SRM drive system has faults (open-circuit or short circuit) in solid state devices or phase windings, the fault tolerance strategy will be triggered. By using the proposed fault tolerance operation strategy, the converter can operate with a half part of the faulty phase winding, then

$$\begin{cases} L_{\max}{}' = \frac{1}{2}L_{\max} \\ L_{\min}{}' = \frac{1}{2}L_{\min} \end{cases} \tag{4}$$

where $L_{\min}'$ and $L_{\max}'$ are the minimum and maximum inductances of the faulty phase; $L_{\min}$ and $L_{\max}$ are the minimum and maximum inductances of the healthy phase.

The slope factor of phase inductance in the inductance ascending region in fault-tolerant operation is

$$K_L{}' = \frac{1}{2}\frac{L_{\max}{}' - L_{\min}{}'}{\theta_2-\theta_1} = \frac{1}{2}K_L \tag{5}$$

where θ_1 and θ_2 are the corresponding rotor positions; K_L and K_L' are the phase inductance slope factors in healthy and fault-tolerant operation states, respectively.

In the current-ascending region, the phase current slope in fault-tolerant operation is

$$K_i{}' = \left(\frac{di}{d\theta}\right)' = \frac{U_{in}}{\omega_r \frac{1}{2}L_{\min}} = \frac{2U_{in}}{\omega_r L_{\min}} = 2K_i \tag{6}$$

where K_i and K_i' are the phase current slope factors in the healthy and fault-tolerant operation conditions, respectively.

The peak value of phase current in fault-tolerant operation is

$$i_{max}{}' = \frac{U_{in}}{\omega_r}\frac{\theta_1-\theta_{on}}{\frac{1}{2}L_{\min}} = \frac{U_{in}}{\omega_r}\frac{2(\theta_1-\theta_{on})}{L_{\min}} = 2i_{max} \tag{7}$$

where i_{max}' and i_{max} are the peak values of phase current in healthy and fault-tolerant operation states, respectively; θ_{on} is the turn-on angle; θ_1 is the position where the phase current reaches its peak value.

The SRM average electromagnetic torque of the faulty phase is given by

$$T_{av}{}' = \frac{N_r}{2\pi}\frac{U_{in}{}^2}{\omega_r^2}\left(\theta_{off}-\theta_1\right)\left(\frac{\theta_1-\theta_{on}}{\frac{1}{2}L_{\min}} - \frac{1}{2}\cdot\frac{\theta_{off}-\theta_1}{\frac{1}{2}L_{\max}-\frac{1}{2}L_{\min}}\right) = 2T_{av} \tag{8}$$

where N_r is the number of rotor poles, and T_{av} and T_{av}' are the phase average electromagnetic torques in healthy and fault-tolerant operation conditions, respectively.

According to (7) and (8), the current peak value and the average electromagnetic torque of the faulty phase in fault-tolerant operations are both twice of the values in the healthy condition. However, in a closed-loop system, due to a constant load, the total average electromagnetic torque of SRM is the same as that in the normal condition.

By using the proposed fault tolerance strategy in CCC mode, the faulty part of the phase converter can be blocked and the healthy part can still be employed for torque output. Because controlling the phase current is the target in CCC mode, the phase current will be regulated to the same reference value as that in the healthy phase. By using the proposed fault tolerance strategy in voltage-PWM control mode, the phase voltage is to be controlled. Aiming at lowering the unbalanced phase current, the turn-on angle of the faulty phase can be adjusted to reduce the influence of unbalanced phase current in the faulty winding. Therefore, the proposed tri-port converter can be employed to compensate and balance the current and torque; and the torque ripple can be reduced to improve the SRM drive performance under fault conditions.

In the open circuit condition, only half the phase winding can be employed to generate torque that will decrease the output torque of SRM in heavy load condition. However, by CCC, the performance of the fault tolerance operation can be the same as the healthy condition when the load is light.

V. SIMULATION AND EXPERIMENT VERIFICATION

In order to validate the proposed tri-port converter for an SRM based HEV, simulation studies and experiments are adopted to verify the proposed topology. A 750W 12/8 SRM with the proposed tri-port converter is modeled in Matlab/Simulink. Fig. 13 presents the simulation results in the voltage-PWM control mode at 500 r/min under normal, power source switching, faulty and fault-tolerant conditions. The turn-on angle of SRM is 0° and the turn-off angle of SRM is 20°, and the load torque is 1 N·m. In the waveforms, T and T^* are the instantaneous torque and given load torque, respectively; i_a, i_b, and i_c represent the three-phase currents, respectively. In the normal state, the three-phase currents have the same shape with 15° phase-shift from each other, and the total torque is the sum of the three-phase torques, as shown in Fig. 13 (a). Fig. 13 (b) shows the power source switching conditions that switch from the battery bank power supply to battery bank and generator supply. The motor system operates steadily when the power supply changes from the battery to the dual source.

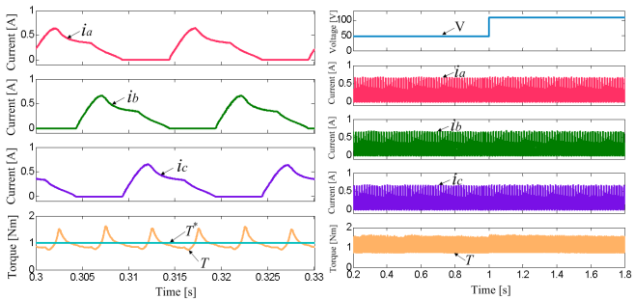

(a) Normal *(b) Power source switching*

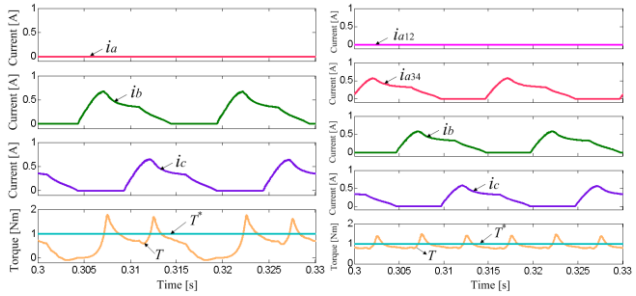

(c) Open fault *(d) Fault-tolerance*

FIGURE 13. Simulation results in voltage-PWM control mode under normal, power supply switching, faulty and fault-tolerant conditions

Fig.13 (c) illustrates the faulty condition of SRM, in which phase-A suffers from an open-circuit fault and the phase current reduces to zero. Due to the independence of each phase, the other normal phases will not be affected by the faulty phase. While by increasing the PWM duty-cycle, the currents in the other healthy phases are excited to be larger than the previous one to compensate the torque loss. However, due to the absence of phase-A torque, the torque ripple is larger than that in normal conditions, as presented in Fig. 13 (c). Fig. 13(d) shows the voltage-PWM control mode under fault tolerance control in faulty conditions. The relay J_1 is switched on when an open-fault is detected in the upper-switch S_1. By passing the phase-A winding L_{a12}, L_{a34} still can be employed for fault tolerance control under this condition, and the torque ripple is obviously reduced compared to that in Fig. 13 (c).

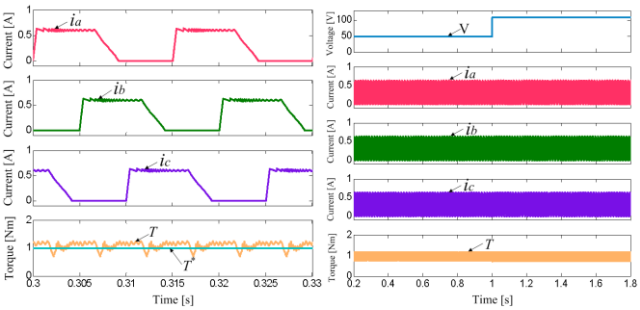

(a) Normal *(b) Power source switching*

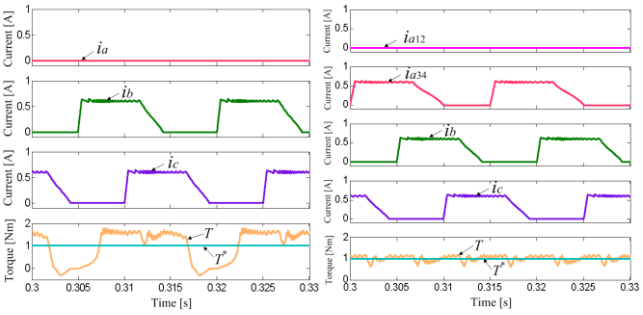

(c) Open fault *(d) Fault-tolerance*

FIGURE 14. Simulation results in current regulation control mode under normal, power supply switching, faulty and fault-tolerant conditions

Fig. 14 shows the CCC mode under normal, power supply switching fault and fault-tolerant conditions. In Fig. 14 (a), the torque ripple is smaller than that of voltage-PWM control mode in the normal condition. Fig. 14 (b) shows the simulation results in power source exchange conditions. When the power supply changes from the battery to dual source in this control mode, the SRM system still operates steadily without obvious fluctuation. The torque ripple is increased obviously under fault conditions, which is similar to the voltage-PWM control mode, as shown in Fig. 14 (c). Fig. 14 (d) presents the fault tolerance that results in CCC mode at 500 r/min. The torque ripple is obviously reduced to the normal state as compared to Fig. 14 (c) by using the proposed topology.

To verify the effectiveness of the proposed tri-port converter for HEV, an experimental rig for testing a three-phase 12/8 prototype SRM driving system is built, as presented in Fig. 15. Table I gives the main motor parameters. The central tapped winding nodes are created and pulled out at the terminals when manufacturing the prototype motor. In the experiment rig, the solid-state devices types are FDA59N30 for MOSFET and IDW75E60 for diode. A dSPACE 1006 platform is adopted to actualize the control algorithm. A magnetic brake is used as the load with 1 N·m torque. An 80 V dc power supply and a 48 V lead-acid battery are employed in the motor drive.

TABLE I
SRM PARAMETERS

Parameters	Value
Phase number	3
Stator poles	12
Rotor poles	8
Rated speed	1500 r/min
Rated power	750 W
Phase resistor	3.01 Ω
Minimum phase inductance	27.2 mH
Maximum phase inductance	256.7 mH
Rotor outer diameter	55 mm
Rotor inner diameter	30 mm
Stator outer diameter	102.5 mm
Stator inner diameter	55.5 mm
Core length	80 mm
Stator arc angle	14°
Rotor arc angle	16°

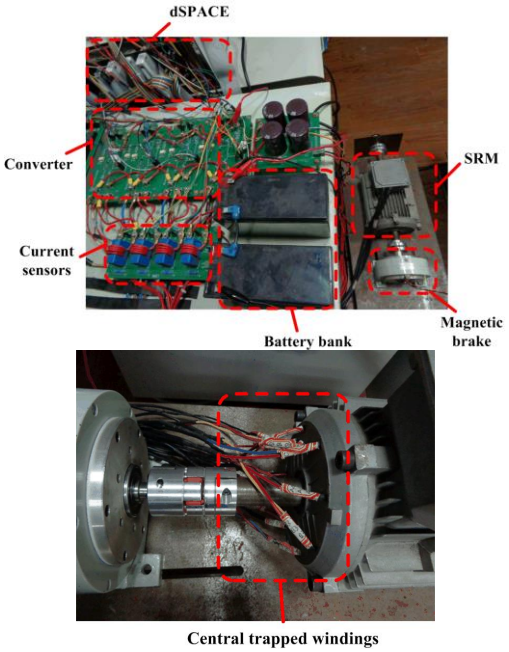

FIGURE 15. Experiment setup

Figs. 16-17 present the experimental results of the three-phase 12/8 SRM at 500 r/min, where the turn-on angle is 0° and turn-off angle is 20°. Fig. 16 (a) shows the experiment results in power source exchange conditions when the power supply changes from the battery to the dual sources, and the motor system operates steadily with limited fluctuations. When SRM is under the healthy condition, three-phase currents are with the same shape and amplitude, as shown in Fig. 16 (b). When the SRM driving system is under one phase open-circuit fault without fault tolerance control, there is no current in the faulty phase. The healthy phase currents are larger than the previous one, as illustrated in Fig. 16 (c). Due to the absence of phase A, the output torque is large than that in the normal condition. A large torque ripple increases the mechanical vibration that may decrease the whole power train system reliability. Fig. 16 (d) verifies the fault tolerance strategy under one phase fault condition. By employing a half part of phase-A winding, the operation of absent phase can be avoided and the SRM output torque ripple can be decreased obviously.

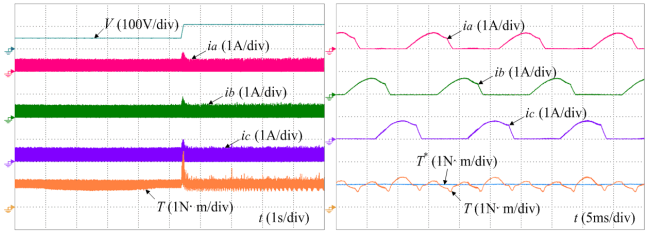

(a) Power source exchange ***(b) Normal***

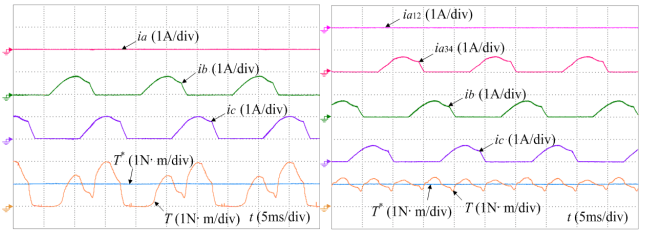

(c) Open fault ***(d) Fault-tolerance***

FIGURE 16. Experiment results in voltage-PWM control mode under power supply switching, normal, faulty and fault-tolerant conditions

Fig. 17 presents the typical waveforms for the CCC system under normal, faulty and fault-tolerant conditions. When the power supply changes from the battery to the dual source, the motor system still can be easily controlled without significant fluctuations, as shown in Fig. 17 (a). Fig. 17 (b) shows the experimental waveforms under the normal condition. In the open-circuit fault condition, there is no current in the faulty phase, and the torque ripple increases significantly, as shown in Fig. 17 (c). By the proposed topology and fault tolerance strategy, the faulty phase can still work and follow the reference current as the healthy phases under CCC mode, as illustrated in Fig.17 (d).

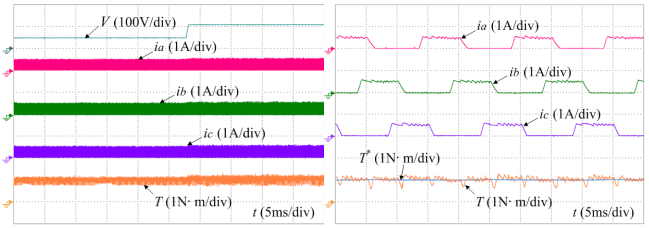

(a) Power source exchange ***(b) Normal***

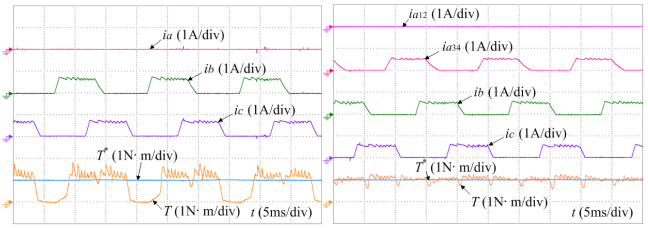

(c) Open fault ***(d) Fault-tolerance***

FIGURE 17. Experiment results in current regulation control mode under power supply switching, normal, faulty and fault-tolerant conditions

The proposed fault tolerance also can work under heavy load conditions, as shown in Fig. 18. When SRM works at 500 r/min with the load of 5 N·m, Fig. 18 (a) displays the fault tolerance operation waveforms in the voltage-PWM control mode under phase-A open-circuit fault. The faulty part of phase converter is blocked (i_{a12}=0), while the healthy part of phase converter still can operate. By adjusting the turn-on angle, the current i_{a34} has the same amplitude as that in the normal phase. Fig. 18 (b) is the fault tolerance operation waveform in CCC control mode under phase-A

open-circuit fault condition. By CCC, i_{a34} has the same amplitude as that in the normal phase. According to the waveform of output torque, the proposed fault tolerance control can limit the torque ripple successfully.

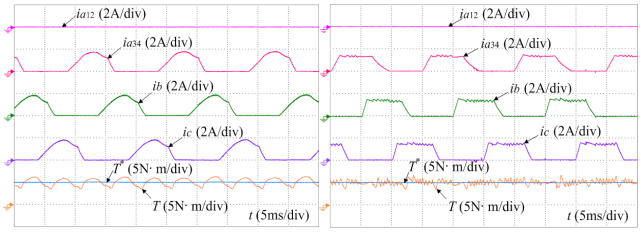

(a) Voltage-PWM control mode (b) CCC mode

FIGURE 18. Experiment results under the heavy load

Fig. 19 illustrates the operation of the proposed SRM driving system during acceleration, high speed operation and load increasing with 1 N·m load. As shown in Fig. 19(a), the real-time speed follows the command well when the speed increases. The proposed fault tolerance strategy can still work for the proposed tri-port converter, as shown in Fig. 19(b). Fig. 19(c) presents the transient process in the load increasing condition, and the speed can still be easily controlled at the command value.

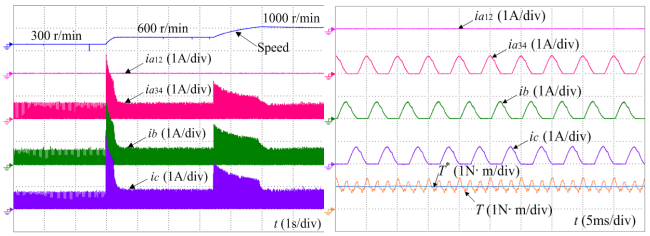

(a) Acceleration (b) Operation at 1500 r/min

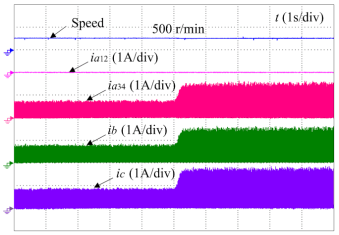

(c) Load increasing

FIGURE 19. Experiment results of fault tolerant operation during acceleration, high speed operation and load increasing

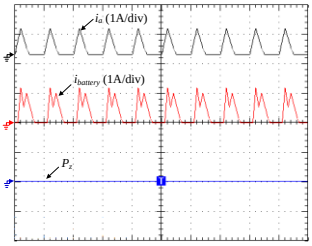

FIGURE 20. Generator charging battery bank

Fig. 20 shows the experiment results of the generator supplying energy to the battery bank, in which $i_{battery}$ is the battery bank charging current, P_z stands for the position sensor signal. Three phase windings are employed to improve charging power. As shown in Fig. 20, P_z is zero during the charging progress, indicating that the SRM is in the standstill condition.

VI. CONCLUSION

SRM has been employed as the motor for HEV application in this paper. In order to achieve flexible energy control for HEV, this paper proposed a tri-port converter with modular and concise structure to combine a generator, a battery bank and an SRM in one converter; and the corresponding working modes, control strategy and fault tolerance operation are investigated. The main contributions of this paper are:

(i) A novel tri-port converter for HEV is proposed that supports flexible energy flow control. Under the driving condition, the proposed topology supports five energy flow modes including generator to SRM, battery bank to SRM, generator and battery bank to SRM, generator to SRM and battery bank, and battery bank to SRM and generator. Under the standstill condition, the proposed topology supports two energy flow modes, namely generator to battery bank, and battery bank to generator modes.

(ii) In order to cooperate with the six working modes, the corresponding control strategies are proposed to achieve flexible energy control.

(iii) The fault tolerance operation and strategies of the proposed topology are studied to expand the proposed topology function.

By deploying the proposed tri-port converter for SRM based HEV system, the topology with a modular structure can be massively produced and supports all six working modes in one converter. Furthermore, the proposed system also can support fault diagnosis and fault-tolerant operation. In more-electric ships and airplanes, the proposed tri-port converter also can be applied to achieve high power density, high reliability and flexible energy flow.

REFERENCES

[1] B. K. Bose, "Global energy scenario and impact of power electronics in 21st century," *IEEE Trans. Industrial Electronics*, vol. 60, no. 7, pp. 2638-2651, Jul. 2013.

[2] Y. Hu, X. Song, W. Cao, and B. Ji, "New SR drive with integrated charging capacity for plug-in hybrid electric vehicles (PHEVs)," *IEEE Trans. Industrial Electronics*, vol. 61, no. 10, pp. 5722-5731, Oct. 2014.

[3] B. Ji, X. Song, W. Cao, V. Pickert, Y. Hu, J. W. Mackersie, and G. Pierce, "In situ diagnostics and prognostics of solder fatigue in IGBT modules for electric vehicle drives," *IEEE Trans. Power Electron.*, vol. 30, no. 3, pp. 1535-1543, Mar. 2015.

[4] S. Morimoto, O. Shohei, Y. Inoue, and M. Sanada, "Experimental evaluation of a rare-earth-free PMASynRM with ferrite magnets for automotive applications," *IEEE Trans. Ind. Electron.*, vol. 61, no. 10, pp. 5749-5756, Oct. 2014.

[5] J. Zhao, P. Zheng, C. Tong, R. Liu, Y. Sui, S. Cheng, and J. Bai, "Experimental study of compound-structure permanent-magnet synchronous machine used for HEVs," *IEEE Trans. Magn.*, vol. 49, no. 2, pp. 807-810, Nov. 2013.

[6] L. Tang, and G. J. Su, "High-performance control of two three-phase permanent-magnet synchronous machines in an integrated drive for

automotive applications," *IEEE Trans. Power Electron.*, vol. 23, no. 6, pp. 3047-3055, Nov. 2008.
[7] A. V. Sant, V. Khadkikar, W. Xiao, and H. H. Zeineldin, "Four-axis vector-controlled dual-rotor PMSM for plug-in electric vehicles," *IEEE Trans. Ind. Electron.*, vol. 62, no. 5, pp. 3202-3212, May 2015.
[8] Y. S. Lai., W. T. Lee, Y. K. Lin, and J. F. Tsai, "Integrated inverter/converter circuit and control technique of motor drives with dual-mode control for EV/HEV applications," *IEEE Trans. Power Electron.*, vol. 29, no. 3, pp. 1358-1365, Mar. 2014.
[9] O. C. Onar, J. Kobayashi, and A. Khaligh, "A fully directional universal power electronic interface for EV, HEV, and PHEV applications," *IEEE Trans. Power Electron.*, vol. 28, no. 12, pp. 5489-5498, Dec. 2013.
[10] I. Boldea, L. N. Tutelea, L. Parsa, and D. Dorrell, "Automotive electric propulsion systems with reduced or no permanent magnets: an overview," *IEEE Trans. Ind. Electron.*, vol. 61, no. 10, pp. 5696-5711, Oct. 2014.
[11] K. M. Rahman, B. Fahimi, G. Suresh, A. V. Rajarathnam, and M. Ehsani, "Advantages of switched reluctance motor applications to EV and HEV: design and control issues," *IEEE Trans. Ind. Appl.*, vol. 36, no. 1, pp. 111-121, Jan./Feb. 2000.
[12] Qin Lei, Dong Cao, and Fang Zheng Peng,"Novel Loss and Harmonic Minimized Vector Modulation for a Current-Fed Quasi-Z-Source Inverter in HEV Motor Drive Application," *IEEE Trans. Power Electron.*, vol. 29, no. 3, pp. 1344-1357, Mar. 2014.
[13] M. A. Khan, I. Husain, and Y. Sozer, "Integrated electric motor drive and power electronics for bidirectional power flow between the electric vehicle and DC or AC grid," *IEEE Trans. Power Electron.*, vol. 28, no. 12, pp. 5774-5783, Dec. 2013.
[14] L. Xu, Y. Zhang, and X. Wen, "Multioperational Modes and Control Strategies of Dual-Mechanical-Port Machine for Hybrid Electrical Vehicles," *IEEE Trans. Ind. Appl.*, vol. 45, no. 2, pp. 747-745, Mar/Apr. 2009.
[15] Miller T. J. E. "Switched reluctance motors and their control," London: Magna Physics Publishing and Oxford Science, 3-25, 1993
[16] X.D.Xue, K.W.E Cheng, T.W. Ng, N.C. Cheung, "Multi-objective optimization design of in-wheel switched reluctance motors in electric vehicles," *IEEE Trans. Ind. Electron.*, vol.57, no.9, pp.2980-2987, Sept. 2010.
[17] J. Ye, B. Bilgin, and A. Emadi, "An extended-speed low-ripple torque control of switched reluctance motor drives," *IEEE Trans. Power Electron.*, vol. 30, no. 3, pp. 1457-1470, Mar. 2015.
[18] K. Kiyota, T. Kakishima, and A. Chiba, "Comparison of test result and design stage prediction of switched reluctance motor competitive with 60-kW rare-earth PM motor," *IEEE Trans. Ind. Electron.*, vol. 61, no. 10, pp. 5712-5721, Oct. 2014.
[19] S. Wang, Q. Zhan, Z. Ma, and L. Zhou, "Implementation of a 50-kW four-phase switched reluctance motor drive system for hybrid electric vehicle," *IEEE Trans. Magn.*, vol. 41, no. 1, pp. 501-504, Jan. 2005.
[20] J. Liang, D. H. Lee, G. Xu, J. W. Ahn, "Analysis of passive boost power converter for three-phase SR drive," *IEEE Trans. Industrial Electronics*, vol. 57, no. 9, pp. 2961-2971, Sep. 2010.
[21] D. H. Lee, T. H. Pham, J. W. Ahn, "Design and operation characteristics of four-two pole high-speed SRM for torque ripple reduction," *IEEE Trans. Industrial Electronics*, vol. 60, no. 9, pp. 3637-3643, Sep. 2013.
[22] L. Shen, J. Wu, and S. Yang, "Initial position estimation in SRM using bootstrap circuit without predefined inductance parameters," *IEEE Trans. Power Electronics*, vol. 26, no. 9, pp. 2449-2456, Sep. 2011.
[23] A. G. Jack, B. C. Mecrow, and J. A. Haylock, "A comparative study of permanent magnet and switched reluctance motors for high-performance fault-tolerant applications," *IEEE Trans. Ind. Appl.*, vol. 32, no. 4, pp. 889-895, Jul/Aug. 1996.
[24] A. K. Jain, and N. Mohan, "SRM power converter for operation with high demagnetization voltage," *IEEE Trans. Ind. Appl.*, vol. 41, no. 5, pp. 1224-1231, Sep./Oct. 2005.
[25] Chai Feng, Pei Yulong, Li Xinmei, Guo Bin, and Cheng Shukang, "The Performance Research of Starter-Generator Based on Reluctance Torque Used in HEV," *IEEE Trans. Magn.*, vol. 45, no. 1, pp. 635-638, Jan, 2009.
[26] C. Hung-Chun, and L. Chang-Ming, "An integrated driving/charging switched reluctance motor drive using three-phase power module," *IEEE Trans. Ind. Electron.*, vol. 58, no. 5, pp. 1763-1775, May 2011.
[27] L. Jianing, L. Dong-Hee, X. Guoqing, and A. Jin-Woo, "Analysis of passive boost power converter for three-phase SR drive," *IEEE Trans. Ind. Electron.*, vol. 57, no. 9, pp. 2961-2971, Sep. 2010.
[28] M. Barnes, and C. Pollock, "Forward converters for dual voltage switched reluctance motor drives," *IEEE Trans. Power Electron.*, vol. 16, no. 1, pp. 83-91, Jan. 2001.
[29] W. K. Thong, and C. Pollock, "Low-cost battery-powered switched reluctance drives with integral battery-charging capability," *IEEE Trans. Ind. Appl.*, vol. 36, no. 6, pp. 1676-1681, Nov./Dec. 2000.
[30] D. H. Lee, and J. W. Ahn, "A novel four-level converter and instantaneous switching angle detector for high speed SRM drive," *IEEE Trans. Power Electron.*, vol. 22, no. 5, pp. 2034-2041, Sep. 2007.
[31] L. Dong-Hee, and A. Jin-Woo, "A novel four-level converter and instantaneous switching angle detector for high speed SRM drive," *IEEE Trans. Power Electron.*, vol. 22, no. 5, pp. 2034-2041, Sep. 2007.